

Received October 14, 2020, accepted October 21, 2020, date of publication October 28, 2020, date of current version November 10, 2020.

Digital Object Identifier 10.1109/ACCESS.2020.3034467

Generation Characteristics Analysis of Deflection Type Double Stator Switched Reluctance Generator

ZHENG LI¹, (Member, IEEE), XUZE YU¹, ZHE QIAN², (Member, IEEE), XUETING WANG¹, YU XIAO¹, AND HEXU SUN¹, (Senior Member, IEEE)

¹School of Electrical Engineering, Hebei University of Science and Technology, Shijiazhuang 050018, China

²School of Electrical Engineering and Automation, Anhui University, Hefei 230601, China

Corresponding authors: Zheng Li (lzhfgd@163.com) and Hexu Sun (hxsun@hebust.edu.cn)


This work was supported in part by the National Natural Science Foundation of China under Grant 51877070, Grant 51577048, and Grant 51637001; in part by the Natural Science Foundation of Hebei Province of China under Grant E2018208155; in part by the Talent Engineering Training Support Project of Hebei Province under Grant A201905008; in part by the National Engineering Laboratory of Energy-Saving Motor and Control Technique, Anhui University, under Grant KFKT201901; and in part by the Hebei Province Higher Education Science and Technology Research Key Project under Grant ZD2018228.

ABSTRACT This article presents the design and operation of a deflection type double stator switched reluctance generator (DDSRG) for wind turbine applications. The DDSRG can generate electricity with high efficiency according to the different wind directions. A deflectable SRG model is proposed to achieve the above requirements, which can deflect in space with different wind directions. First, this article introduces the special structure of the DDSRG. And the operating principle of DDSRG with special structure is explained. At the same time, the mathematical model of the external generator is built as an example. The voltage characteristics of DDSRG under different wind conditions such as directions, wind speeds, and deflection angles are studied. The comparison between the analytical method and the finite element method verifies the accuracy of the theory. Finally, the proposed DDSRG is tested to verify its power generation characteristics.

INDEX TERMS Deflection, double stator, efficiency, generator, SRG.

FREQUENTLY USED SYMBOLS

α_i	Angle of incidence	g	Air gap interval
β_i	Angle of refraction	N_s	Number of stator poles
μ_1	Rotor permeability	N_r	Number of rotor poles
μ_2	Permeability of magnetic isolation material	β_s	Pole arc of stator
δ_i	Air gap lengths	β_r	Pole arc of rotor
L	Inductance of the generator	h_{cs1}	Yoke height of outer stator
θ_i	Rotor position angle	h_{cs2}	Yoke height of internal stator
U_a	A-phase voltage	h_{cr}	Yoke height of rotor
E_a	A-phase winding potential	l_a	Length of core
i_a	A-phase winding phase current	α	Range of rotor deflection
R_a	A-phase winding resistance	A_{cd}	Rated current density
ψ_a	A-phase flux linkage	n_N	Rated rotation speed
ω	Angular velocity	P_N	Rated power
N	Number of turns per phase	T_N	Rated rotating torque
D_{s1}	Outer radius of outer stator	U_N	Rated voltage
D_{s2}	Inner radius of inner stator	h_i	Thickness of magnetic isolation
D_{r1}	Outer radius of rotor	ξ	Integral difference
D_{r2}	Inner radius of rotor	U_{EXP}	Voltage value measured by the experimental data
		U_{AM}	Voltage value measured by analytical method
		W_G	Generator energy
		η_1	Wind energy

The associate editor coordinating the review of this manuscript and approving it for publication was Christopher H. T. Lee .

W_w Conversion efficiency
 γ Wind direction Angle

I. INTRODUCTION

As a new concept of motors, it has appeared for nearly five decades. Switched reluctance motor has the characteristics of simple structure, reliable operation, high torque and high efficiency. It is widely used in important fields such as electric vehicles, textile industry and coke industry [1], [2]. With the advancement of technology and manufacturing process. Many prototype models of switched reluctance generations have been manufactured and studied. References [3]–[9]. These proposed switched reluctance motors have different structures and can be used for various purposes. Most of these proposed motors are used for special purposes. Therefore, their energy conversion rate is not very good. This is also the existing shortcoming of the switched reluctance motor.

Compared with single stator generators, double stator generators have better efficiency [10]–[12]. At the same time, the switched reluctance motor with double stator structure also has higher accuracy and better material utilization [13]. The double stator structure will inevitably increase the loss of the motor, which is also a problem that needs attention [14].

At present, many switched reluctance generators are combined with wind power generation [15]–[18]. Usually, the wind direction will affect the efficiency of the generator. When the energy of the wind is fixed and the angle of deviation between the wind and the turbine is increased, the energy obtained by the generator will obviously decrease. When the angle between the wind and the turbine is too large, the generator will not be able to provide enough power supply to the outside. Many optimization methods for switched reluctance motors are mentioned in the references [19]–[24], but these methods have their own limitations, and in many cases where the wind direction is unstable, the efficiency of power generation cannot be effectively improved. In order to improve the power generation efficiency of the generator, this article combines the concept of multiple degrees of freedom with the generator. Most existing multi-DOF motors are motor structures [25]–[30]. If the angle of the rotating blades can be deflected to a certain extent, the efficiency of the generator will inevitably be improved.

Compared with the traditional SRG, this structure has the better accuracy and response speed. At the same time, it can achieve greater efficiency utilization of wind energy by adjusting the deflection angle and has better energy utilization effect compared with the non-deflection SRG. The SRG proposed in this article has the capability of spatial deflection, and the deflection angle can be adjusted by detecting the external wind direction to achieve true high-efficiency operation. This deflectable structure greatly improves the power generation efficiency of SRG, which has very important significance for the future wind power generation system.

At present, the optimization of generators is centered on how to improve their work efficiency. Efficient generators can

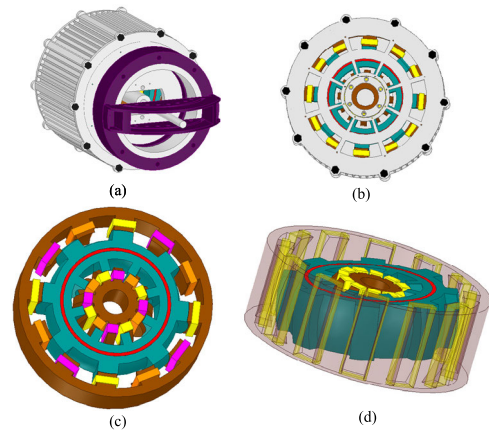


FIGURE 1. Schematic diagram of generator (a) Entity drawing, (b) Schematic diagram of bottom, (c) Internal structure of double stator generator, (d) Rotor deflection diagram.

save a lot of resources. Inefficient generators waste a lot of social resources. If the efficiency of all generators can now be increased by 5%, the annual electricity savings will exceed 5.4 billion kWh. The saved energy is re-integrated and used in other fields, avoiding unnecessary waste.

In this article, a DDSRG is proposed. DDSRG integrates the concept of generator and multi-degree of freedom. The multi-degree of freedom of the generator makes it possible to improve the efficiency. Especially in the harsh environment and frequent wind direction changes, DDSRG can effectively improve the power generation efficiency.

The research shows that the deflection type double stator switched reluctance generator proposed in this article can effectively improve the efficiency of power generation. It can be verified through experiments that the efficiency of the generator is increased by 5~8% every time the wind direction and turbine offset angle are reduced by 5°.

II. TOPOLOGY AND WORKING PRINCIPLE

A. BASIC STRUCTURE

Fig. 1 shows the schematic diagram of four different states of the deflection type double stator switched reluctance generator, in which Fig. 1. (a) shows the appearance of the generator entity, Fig. 1. (b) shows the bottom of the entity. Fig. 1. (a) and Fig. 1. (b) can well show the appearance of the SRG. Fig. 1. (c) shows the internal structure diagram of the double stator generator, and it can also show the state diagram of the generator at a certain moment of rotation. Fig. 1. (d) shows the internal structure diagram of the motor when the rotor deflects. Fig. 1. (c) and Fig. 1. (d) can well show that the SRG is in two states of rotation and deflection.

Fig. 2 shows the structure of the deflection type double stator SRG, which consists of a measuring device, fixing device, bearing, shell and internal motor. The measuring device can detect the motion state of the rotor and judge whether the rotor is in rotation or deflection. The fixed device is the guarantee of the stable operation of the motor. One side of the bearing is connected with the rotor. When the shaft is driven by an external force, it can drive the rotor to move in

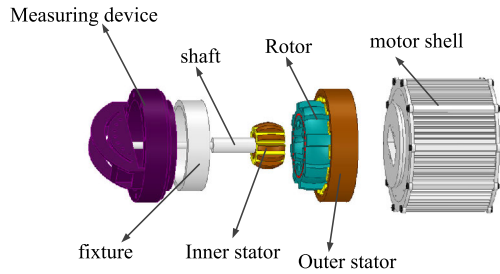


FIGURE 2. Structure of deflection type double stator switched reluctance generator.

TABLE 1. Main specifications of the generator.

Parameter	Quantity	Size
N	Number of turns per phase	200
D_{s1}	outer radius of outer stator	300mm
D_{s2}	Inner radius of inner stator	13.5mm
D_{r1}	outer radius of rotor	108mm
D_{r2}	inner radius of rotor	43.3mm
g	air gap interval	2mm
N_s	number of stator poles	12
N_r	number of rotor poles	8
β_s	pole arc of stator	15
β_r	pole arc of rotor	16.2
h_{cs1}	yoke height of outer stator	13.5mm
h_{cs2}	yoke height of internal stator	11.5mm
h_{cr}	yoke height of rotor	16mm
l_a	length of core	90mm
α	range of rotor deflection	0~17°
A_{cd}	Rated current density	6A/mm ²
n_N	Rated rotation speed	200r/min
P_N	Rated power	2.5kW
T_N	Rated rotating torque	70N·m
U_N	Rated voltage	380V
h_i	Thickness of magnetic isolation	15mm

the same state. The shell can protect the internal motor and the shell is also an indispensable part of the motor.

The inside of the deflection type double stator switched reluctance generator is mainly composed of three parts: the inner stator, the outer stator and the rotor. The two stators are distributed with centralized windings, which are connected with the outer circuit. When the energy is converted, the conversion from mechanical energy to electrical energy can be realized.

The generator’s parameters are shown in Table 1.

B. PRINCIPLE OF GENERATOR

The deflection type double stator SRG can be regarded as two different SRGs: internal SRG and external SRG. When the rotor is driven by an external force, the rotor position sensor collects the rotor position and realizes excitation and continuous current generation through closed-loop control.

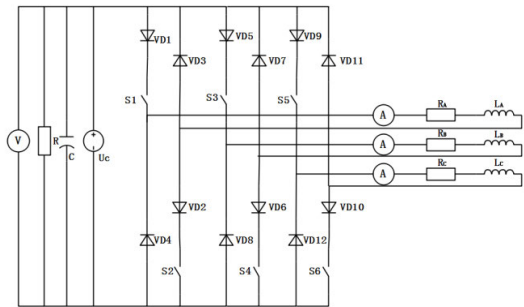


FIGURE 3. Generator control circuit diagram.

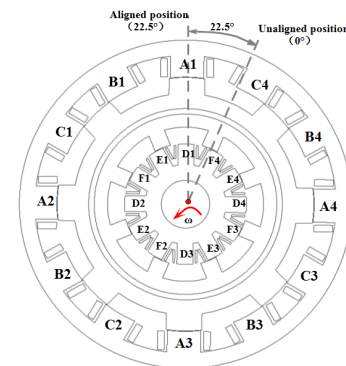


FIGURE 4. Section diagram of generator.

The power generation principle is similar to that of general switched reluctance generator. Due to the page limitation, there is no need to elaborate on it in detail.

Unlike the traditional SRG, the deflection SRG adopts an internal and external double stator structure, so the control circuit can be connected with the external stator and the inner stator by two sets of equipment. It can be considered that the outer stator winding is divided into three phases A, B and C, and the inner stator winding is divided into three phases D, E and F to form two sets of external control circuits.

Fig. 3. shows the control circuit diagram of the generator. The control circuit is mainly composed of the following parts: diode, conduction switch, excitation voltage source, etc. The diode is responsible for power supply and continuous current, and the conduction switch is responsible for driving and controlling the generator.

Fig. 4. shows the cross-section of the generator, with the corresponding angle and phase number distribution of the two parts of the winding marked.

C. MAGNETIC SHIELDING CHARACTERISTIC

It is worth mentioning that a special “magnetic shield” (magnetic separator) is provided on the rotor. This “magnetic shield” is different from the silicon steel plate used in the rotor stator. It is a material with a very low permeability. “Magnetic shielding” can well separate the magnetic field generated by the inner and outer stators, avoid magnetic field interference, and have a positive effect on the generator’s power generation characteristics.

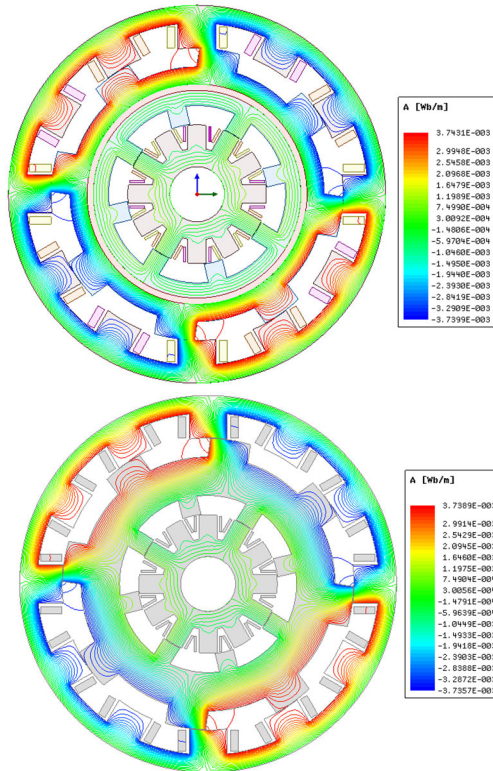


FIGURE 5. Effect of magnetic shielding on magnetic field line.

Fig. 5 shows the influence of “magnetic shielding” on the magnetic field line in the rotor. It can be seen from the figure that the inner teeth and outer teeth of the magnetic field line of the rotor without “magnetic shielding” will interfere with each other, and the magnetic field line formed between the inner teeth and the outer teeth of the rotor with “magnetic shielding” structure will cycle within its own tooth range, so as to achieve the purpose of magnetic shielding.

In Fig. 5, there is a certain interval between the stator and the rotor, and the magnetic line of force is transmitted through the air gap between the rotor and the stator.

The four angles marked at the interface meet the following formula:

$$\frac{\tan \alpha_i}{\tan \beta_i} = \frac{\mu_2}{\mu_1} \quad (1)$$

where α_i and β_i are the angles shown in Fig. 6, $i = 1, 2$.

When the magnetic permeability of the two kinds of materials is different, the magnetic lines of force will be refracted to a greater extent when passing through the interface, and will be biased toward the material with the larger magnetic permeability. According to formula (1), it can be known that the magnetic field connection between the inner and outer stators can be effectively cut only by selecting a magnetic isolation material with a small magnetic permeability to achieve the purpose of isolating the magnetic field.

Fig. 7. (a) shows the rotor stress distribution during three-phase power generation, and Fig. 7. (b) shows the stress distribution during three-phase power generation. Fig. 7. (c) shows the relationship between the average stress and thickness on the magnetic isolation ring during

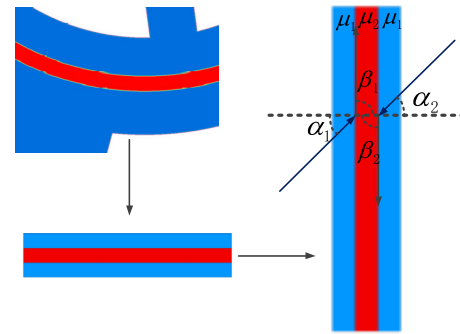


FIGURE 6. Schematic diagram of “magnetic shielding” interface.

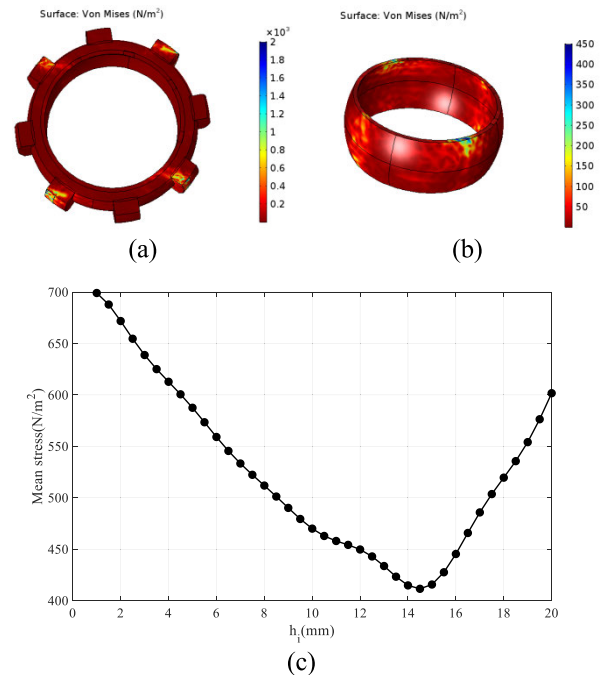


FIGURE 7. Analysis of the stress.

three-phase power generation. As the magnetic isolation thickness increases from zero, the average stress gradually decreases from 699.82 N/m². When the magnetic isolation thickness reaches 15 mm, the average stress reaches a minimum of 402.15 N/m². When the magnetic isolation thickness increases, the average stress gradually increases.

(a) the rotor stress distribution during three-phase power generation (b) the stress distribution during three-phase power generation, (c) the relationship between the average stress and thickness on the magnetic isolation ring during three-phase power generation

Fig. 8. is a temperature distribution diagram of a generator. It can be seen from the figure that the electric heating part is mainly concentrated on the internal and external stators. The heat dissipation space of the inner stator is relatively small, so the temperature is high, while the heat dissipation space of the outer stator is large, so the temperature is low. This temperature distribution does not change much under deflection.

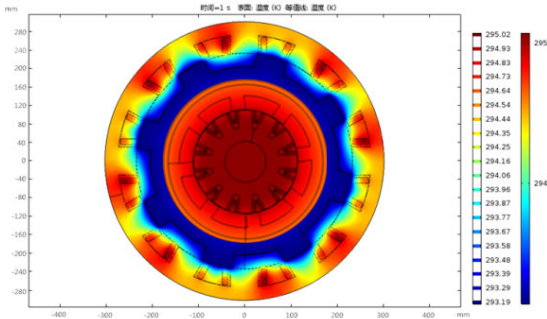


FIGURE 8. Temperature distribution of generator.

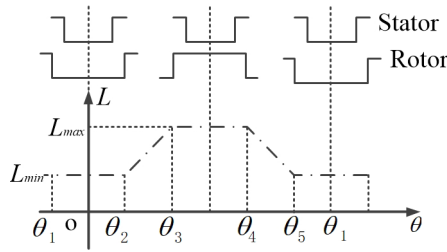


FIGURE 9. Relationship between inductance and rotor position.

III. ANALYSIS OF GENERATOR MATHEMATICAL MODEL, AIR GAP, IRON CONSUMPTION AND EFFICIENCY

A. ANALYSIS OF GENERATOR INDUCTANCE

The voltage and current generated by the deflection type double stator switched reluctance generator are closely related to the inductance value. Therefore, firstly, the inductance of the generator is analyzed. Formula (2) points out several different expressions of the inductance at different conduction angles. The significance of the conduction angle can be obtained from Fig. 9.

$$L(\theta) = \begin{cases} L_{min} & \theta_1 \leq \theta \leq \theta_2 \\ \frac{(L_{max} - L_{min})(\theta - \theta_2)}{\theta_3 - \theta_2} + L_{min} & \theta_2 \leq \theta \leq \theta_3 \\ L_{max} & \theta_3 \leq \theta \leq \theta_4 \\ L_{max} - \frac{(L_{max} - L_{min})(\theta - \theta_4)}{\theta_3 - \theta_2} & \theta_4 \leq \theta \leq \theta_5 \end{cases} \quad (2)$$

where θ_1 is the position where the rotor slot centerline coincides with the stator salient pole centerline. θ_2 is the rotor position angle when the leading edge of the rotor tooth and the leading edge of the stator tooth coincide. θ_3 is the rotor position angle when the leading edge of the generator rotor and the trailing edge of the stator coincide. θ_4 is the rotor position angle when the trailing edge of the rotor coincides with the leading edge of the stator. θ_5 is the rotor position angle when the trailing edge of the rotor tooth pole coincides with the trailing edge of the stator tooth pole.

Next, A-phase will be taken as an example to establish an ideal phase voltage model and analyze it.

When the rotor position angle is θ_{on} or θ_{off} , the generator is in the excitation state, and its voltage equation can be expressed as:

$$U_a = -E_a + i_a R_a \quad (3)$$

where E_a is the A-phase winding potential. i_a is the A-phase winding phase current. R_a is the A-phase winding resistance.

When the rotor position angle $\theta > \theta_{off}$, the generator is in the power generation stage, and the voltage can be expressed as:

$$-U_a = -E_a + i_a R_a \quad (4)$$

The flux linkage of the ideal linear model winding can be expressed as:

$$\psi_a = L i_a \quad (5)$$

Further obtain the corresponding A-phase winding potential:

$$E_a = -\frac{d\psi_a}{dt} = -L \frac{di_a}{dt} - i_a \frac{\partial L}{\partial \theta} \frac{\partial \theta}{\partial t} \quad (6)$$

The voltage equation can be obtained by Equations 4 and 6:

$$\pm U_a = L \frac{di_a}{dt} + i_a \left(\frac{\partial L}{\partial \theta} \frac{\partial \theta}{\partial t} + R_a \right) \quad (7)$$

Ignore the resistance voltage drop across the generator winding:

$$\pm U_a = \frac{d\psi_a}{dt} = \frac{d\psi_a}{d\theta} \frac{d\theta}{dt} = \frac{d\psi_a}{d\theta} \omega \quad (8)$$

where $d\psi_a = \pm \frac{U_a}{\omega} d\theta$

When $\theta_{on} \leq \theta \leq \theta_{off}$ the flux equation can be expressed as:

$$\psi(\theta) = \frac{U_a}{\omega} (\theta - \theta_{on}) \quad (9)$$

When $\theta_{off} \leq \theta \leq 2\theta_{off} - \theta_{on}$ the flux equation can be expressed as:

$$\psi(\theta) = \frac{U_a}{\omega} (2\theta_{off} - \theta_{on} - \theta) \quad (10)$$

B. ANALYSIS OF GENERATOR ELECTROMAGNETIC TORQUE

The electromagnetic torque can be expressed as:

$$T = \begin{cases} 0 & \theta \leq \theta_1 \\ \frac{(L_{max} - L_{min})}{2(\theta_2 - \theta_1)} i^2 & 0 \leq i \leq i_1, \theta_1 \leq \theta \leq \theta_2 \\ \frac{(L_{max} - L_{min})}{2(\theta_2 - \theta_1)} i_1 i & i \geq i_1, \theta_1 \leq \theta \leq \theta_2 \\ 0 & \theta_2 \leq \theta \leq \theta_3 \end{cases} \quad (11)$$

where i_1 is the Critical current.

The inner rotor generator composed of the outer stator and the outer rotor is the main analysis object. Under the ideal linear model, analyze the change law of A, B, C three-phase magnetic flux. The direction from the inner diameter to the outer diameter is the positive direction of the magnetic flux of the stator and rotor tooth poles, and the counterclockwise direction is the positive direction of the magnetic flux of the stator and rotor yoke. Excitation in the order of A-B-C-A, the magnetic flux expression of the outer stator teeth is obtained as:

$$\begin{bmatrix} \Phi_{spA} \\ \Phi_{spB} \\ \Phi_{spC} \end{bmatrix} = - \begin{bmatrix} \Phi_{spA'} \\ \Phi_{spB'} \\ \Phi_{spC'} \end{bmatrix} = \frac{1}{N_{ph}} \begin{bmatrix} 1 & 0 & 0 \\ 0 & -1 & 0 \\ 0 & 0 & 1 \end{bmatrix} \begin{bmatrix} \Psi_A \\ \Psi_B \\ \Psi_C \end{bmatrix} \quad (12)$$

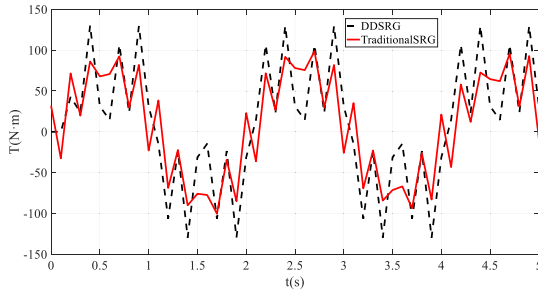


FIGURE 10. Torque comparison.

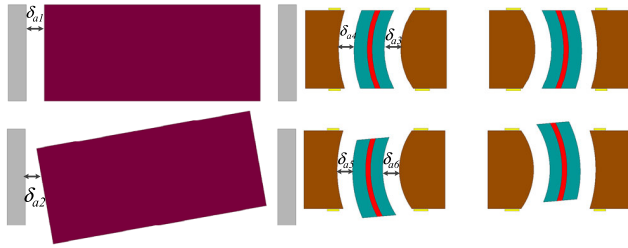


FIGURE 11. Schematic diagram of axial air gap length.

where ψ_A, ψ_B, ψ_C are the flux linkage of each phase winding, $\Phi_{spA}, \Phi_{spB}, \Phi_{spC}$ are the magnetic flux of each phase winding.

The expression of the magnetic flux of the outer stator yoke is

$$\begin{bmatrix} \Phi_{sc1} \\ \Phi_{sc2} \\ \Phi_{sc3} \end{bmatrix} = - \begin{bmatrix} \Phi_{sc1'} \\ \Phi_{sc2'} \\ \Phi_{sc3'} \end{bmatrix} = \frac{1}{2} \begin{bmatrix} 1 & -1 & 1 \\ 1 & -1 & -1 \\ 1 & 1 & -1 \end{bmatrix} \begin{bmatrix} \Phi_{spA} \\ \Phi_{spB} \\ \Phi_{spC} \end{bmatrix} \quad (13)$$

where $\Phi_{spA}, \Phi_{spB}, \Phi_{spC}$ are the magnetic flux of each phase yoke.

Figure 10 shows the torque comparison between DDSRG and traditional SRG. It can be seen from the figure that the torque ripple of DDSRG is large, which is determined by its deflectable structure.

C. ANALYSIS OF GENERATOR AIR GAP ANALYSIS

It can be seen from Fig. 11. that the values of the axial air gap lengths δ_{a1} and δ_{a2} of the conventional cylindrical motor before and after the deflection movement cannot be kept consistent. This situation will cause the axial air gap of the motor to be uneven and affect the performance of the motor. It can be seen from Fig. 11. that the values of the axial air gap length of the generator proposed in this article before and after the deflection movement are $\delta_{a4} = \delta_{a5}$ and $\delta_{a3} = \delta_{a6}$. Obviously, there is no obvious change in the axial length, which is determined by the inner and outer stator and rotor shapes. The inner stator has a spherical outer contour corresponding to the spherical inner contour of the rotor, which can keep the air gap between the inner stator and the rotor constant. Similarly, the outer stator has a spherical inner contour corresponding to the spherical outer contour of the rotor, which can keep the air gap between the outer stator and the rotor constant.

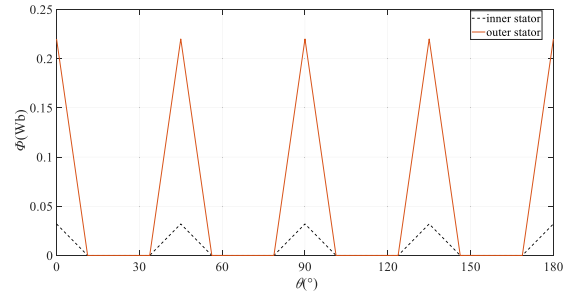


FIGURE 12. Stator tooth flux.

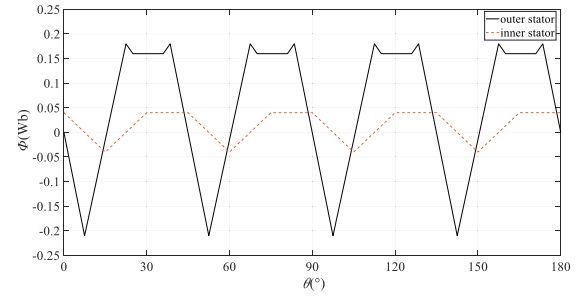


FIGURE 13. Stator yoke flux.

The magnetic flux of the stator teeth is shown in Fig. 12. The magnetic flux of the rotor yoke is shown in Fig. 13.

D. ANALYSIS OF GENERATOR CORE LOSS AND EFFICIENCY

When the generator is in the rotation state, the core loss cannot be directly measured and needs to be obtained indirectly. The expression of the core loss is

$$P_{Fe} = P_1 - P_2 - P_{Cu} - P_{fw} - P_s \quad (14)$$

where P_1 is input power, P_2 is output power, P_{Cu} is copper loss, P_{fw} is mechanical loss and P_s is stray loss. P_1 is a fixed input power. P_2 output power is obtained by testing the output current and voltage. P_{Cu} is obtained by measuring current and resistance. P_s is obtained by empirical formula, so the data obtained by experiment and finite element method are the same. According to the empirical formula, P_{fw} can be expressed as:

$$P_{fw} = 6.5 \left(\frac{3}{p} \right)^2 D_2^3 \quad (15)$$

where p is the number of generator poles and D_2 is the armature diameter.

The finite element software is ANSYS electronics. It can be used to analyze loss and electromagnetism.

In is needed to conduct relevant experimental analysis on iron loss when $n = 50$ rpm, and the data obtained are shown in Table 2 and 3.

Table 2 is the experimental testing result and the comparison of the simulation calculation data, through the prototype test results shows that the generator's core loss calculation error is within the scope of the permit, core loss is verified the correctness of the calculation and optimization scheme. Table 3 shows the loss values.

TABLE 2. Comparison of measured and calculated values of generator iron loss.

area	Experimental measurement	Simulation value
Internal core loss /W	76.08	73.92
External core loss /W	261.62	257.25
Total core loss /W	337.70	331.17

TABLE 3. Loss.

	Outer	Outer	Inner	Inner
	FEM	Experience	FEM	Experience
P_1	1200W	1200W	300W	300W
P_2	834.82W	830.004W	190.949W	188.939W
P_{cu}	60.47W	59.446W	19.731W	19.261W
P_{fw}	11.46W	12.93W	6.4W	6.72W
P_s	36W	36W	9W	9W

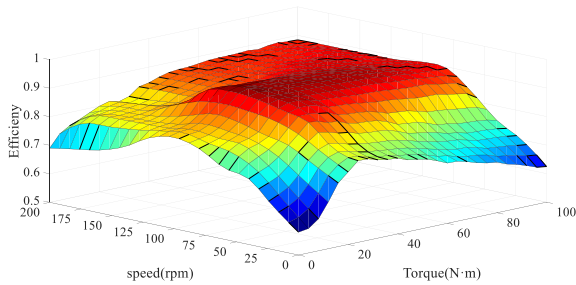


FIGURE 14. Three-dimensional distribution diagram of motor efficiency.

Compared with the traditional switched reluctance generator, the proposed generator has the ability to adjust the deflection angle according to the wind direction. As can be seen from Fig. 1. (d), an offset angle is created between the rotor and the stator. This angle is called the deflection angle. Adjusting the deflection angle with the change of wind direction can make the proposed generator produce higher power generation efficiency than the traditional switched reluctance generator.

Fig. 14. is a three-dimensional distribution diagram of motor efficiency. It can be seen from Fig. 14. that the working efficiency of the proposed generator can be maintained above 0.8 under a wide range of application conditions. Only proper debugging of the generator is needed, and its working efficiency can be maintained at 0.9 or even higher.

IV. ANALYSIS OF THE CHARACTERISTICS OF ROTATING POWER GENERATION

Suppose the prime mover is at nearly constant speed with wind power input, the excitation voltage is constant at 15V, and the average temperature is about 20°. The voltage curves can be obtained by adjusting the speed of the prime mover. Fig. 15. shows the comparison between the experimental data and the analytical method under two different rotating speeds under the generator rotation state, and introduces the concept of “integral difference” to verify the accuracy of the analytical theory.

“Integral difference” is a tool used to judge the deviation of two similar curves. It can be applied to two curves whose periods are approximately the same as the change laws and whose amplitudes are only different. “Integral difference”

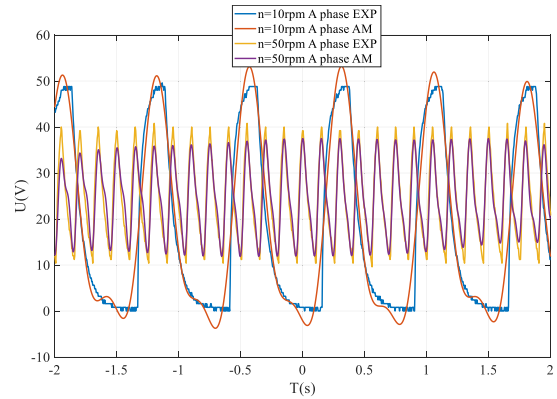


FIGURE 15. Comparison of experimental data and analytical method under two different rotating speeds of generator.

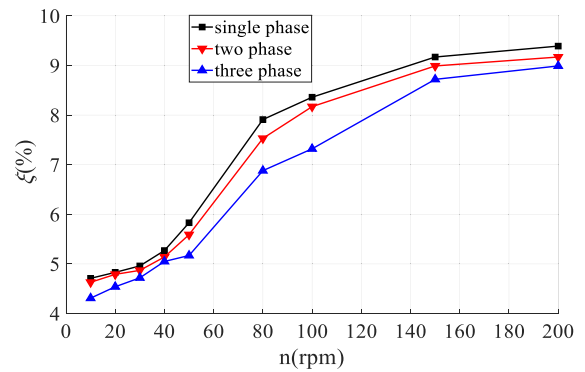


FIGURE 16. “Integral difference” of different rotating speeds under the condition of generator rotation.

can be expressed in the form of formula (16):

$$\xi = \frac{|\int_T |U_{EXP}| dt - \int_T |U_{AM}| dt|}{\int_T |U_{EXP}| dt} \times 100\% \quad (16)$$

where U_{EXP} is the voltage value measured by the experimental data, U_{AM} is the voltage value measured by analytical method, T is a voltage cycle.

The large value of “integral difference” shows that the accuracy of analytical method is low, on the contrary, it shows that the accuracy of analytical method is high.

The single-phase “integral difference” under different rotating speeds is shown in Fig. 16 under the condition of generator rotation.

It can be seen from the figure that as the prime mover speed increases, the “integral difference” also increases.

When the speed increases from 10r/min to 200r/min, the “integral difference” of single phase increases from 4.71% to 9.39%, the “integral difference” of two phase increases from 4.63% to 9.17%, the “integral difference” of three phase increases from 4.31% to 8.99%. but The error is still within the acceptable range. As the number of voltage phases increases, the “integral difference” decreases, so the prediction accuracy of analytical method for multi-phase system is higher.

The single-phase voltage waveform at different speeds is shown in Fig. 17. With the increase of the rotating speed of the

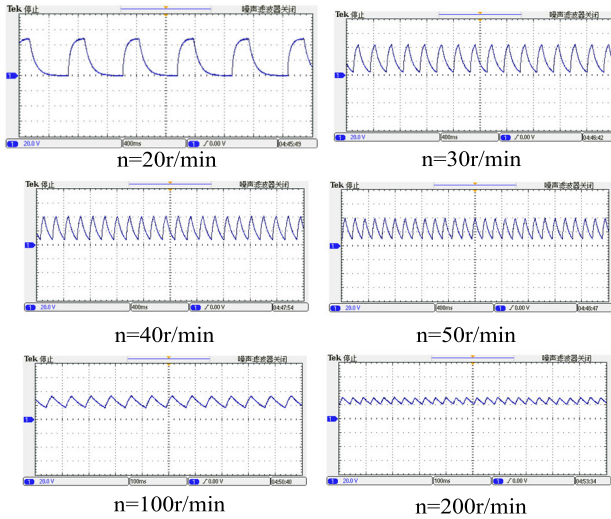


FIGURE 17. Single phase voltage waveform of different rotating speeds under the condition of generator rotation.

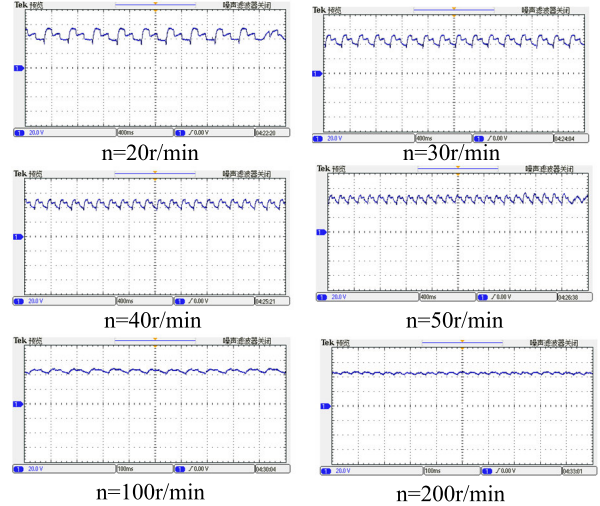


FIGURE 19. Three phase voltage waveforms of different rotating speeds under the condition of generator rotation.

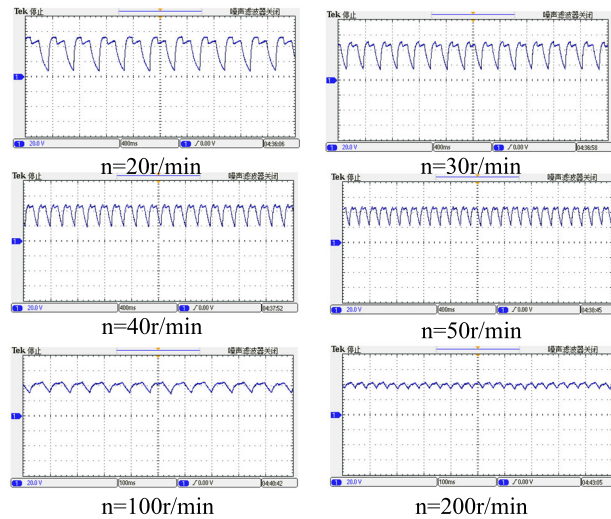


FIGURE 18. Two phase voltage waveforms of different rotating speeds under the condition of generator rotation.

prime mover, the voltage period generated in the same time has been significantly reduced, and the generation frequency has been significantly increased. Fig. 18. and Fig. 19. respectively show the two-phase and three-phase voltage waveforms of different rotating speeds under the condition of generator rotation. The change trend of Fig. 18., Fig. 19. and Fig. 20. is basically the same, and the generation frequency increases significantly with the rotating speed. Fig. 20. shows the experiment platform of rotating voltage test.

V. ANALYSIS OF THE CHARACTERISTICS OF DEFLECTION POWER GENERATION

Fig. 21. decomposes the wind direction along the axial and radial direction into two components, among which the radial component can drive the motor to rotate. so it is desirable to obtain a sufficiently large radial component.

When the wind energy acts on the generator bearing, most of the energy is converted into mechanical energy to push the bearing, and some of the energy is converted into heat

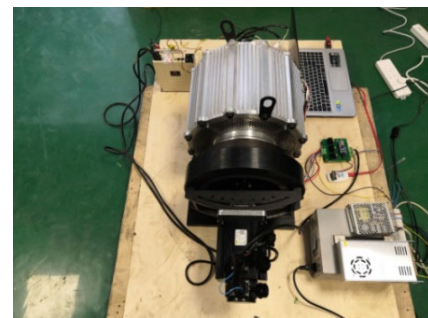


FIGURE 20. The experiment of rotating voltage.

form which cannot be used by the generator. The conversion efficiency model can be equivalent to equation (17):

$$W_G = \eta_1 W_w \tag{17}$$

where W_G is the generator energy. W_w is the wind energy. η_1 is conversion efficiency.

When considering wind direction, formula (17) is expressed as:

$$\eta_1 W_w \cos \gamma = W_G \tag{18}$$

It can be further expressed as:

$$W_G = \eta_2 W_w \tag{19}$$

where $\eta_2 = \eta_1 \cos \gamma$.

Because the wind direction cannot be completely converted into radial component, the wind energy is weakened in two parts, and the actual conversion rate is extremely low, so the power generation effect is greatly limited.

Since the conversion process of wind energy to mechanical energy needs to go through two energy weakening parts, the first part is analyzed to caused by the wind direction is not completely radial, and the second part is a part of thermal energy converted when the wind and the generator bearing rub. The energy loss of the second part cannot be avoided, but the energy loss of the first part can weaken the γ angle through the deflection movement, which can play the

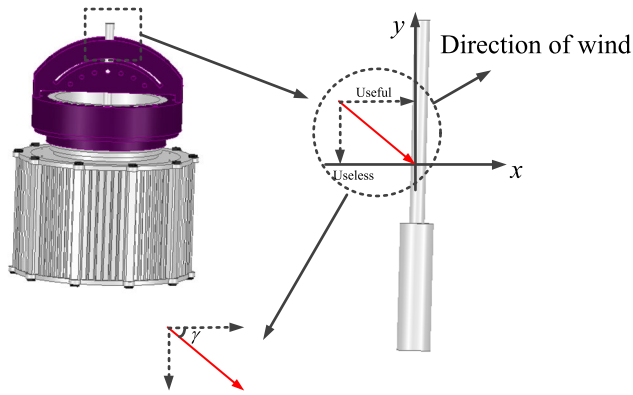


FIGURE 21. Effective component of wind direction.

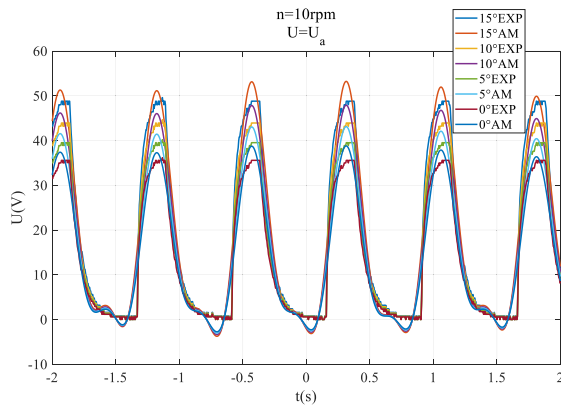


FIGURE 22. Voltage characteristics of different deflection angles when “wind direction” is offset by 15°.

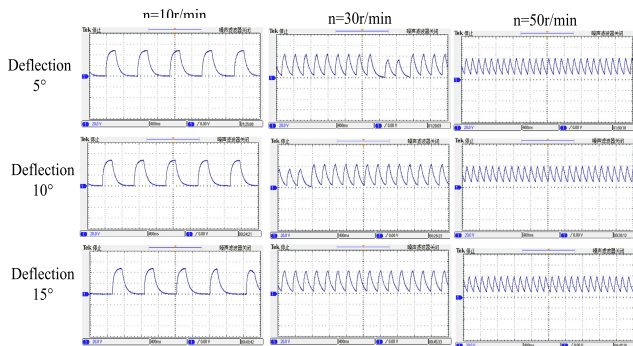


FIGURE 23. Single phase voltage characteristics under different rotating speed and deflection angle.

role of converting the non radial component into the radial component.

After the experimental verification, it is found that there are similar experimental rules for the simulation of other different deflection angles. Here, taking Fig. 22. as an example, it is enough to explain that there is no need to elaborate on other. After the experimental verification, it is found that there are similar experimental laws for other simulation under different deflection angles. Here, take Fig. 22 as an example to illustrate the law of change.

Fig. 23. shows the generation voltage characteristics under different rotating speeds and deflection angles, which are

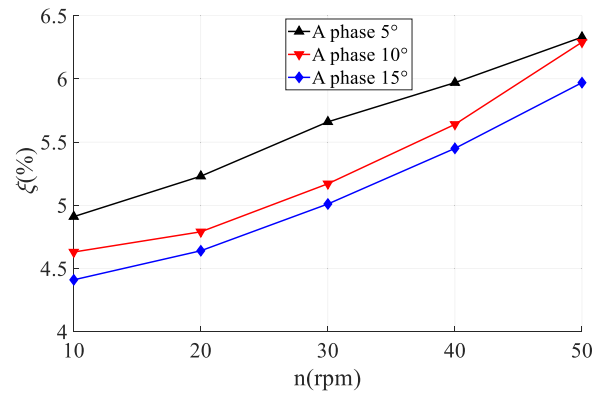


FIGURE 24. “Integral difference” of different deflection degree under the condition of generator.

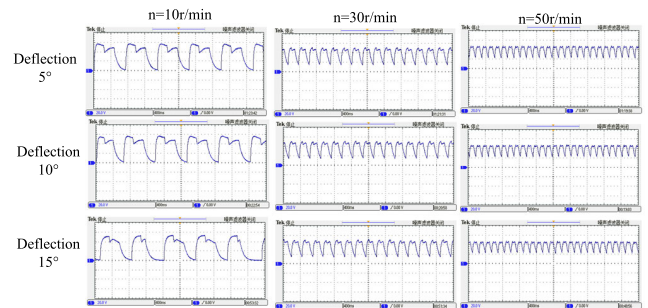


FIGURE 25. Two phase voltage waveforms of different rotating speeds under the condition of generator deflection.

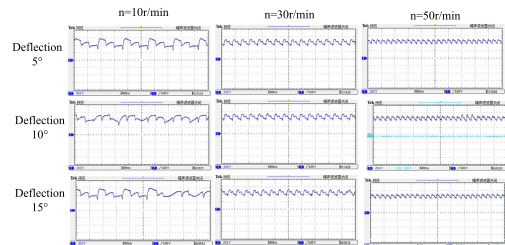


FIGURE 26. Three phase voltage waveforms of different rotating speeds under the condition of generator deflection.

basically consistent with the basic change rule of the rotating generation characteristics, but the amplitude is increased, which can better meet the generation demand under different wind directions. The generator can adjust the deflection angle with the change of wind direction, and the voltage will not increase or decrease significantly with the change of wind direction.

Fig. 24 shows the “integral difference” under three different deflection angles when the single-phase speed $n = 10r/min$. the change trend is similar to that before, and the change is not significant.

Fig. 25. and Fig. 26. show the two-phase and three-phase voltage waveforms of the generator at different rotating speeds and deflection angles, respectively.

Fig. 22. simulates the wind direction with a 15° deviation. The prime mover uses the equivalent torque to test the single-phase voltage of the generator under several different deflection angles. The test results show that the corresponding

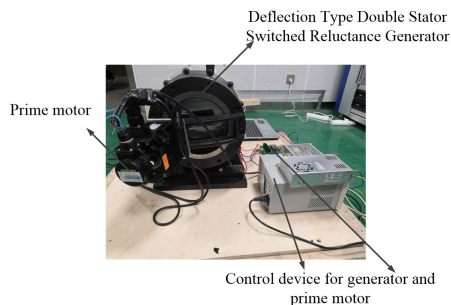


FIGURE 27. The experiment of deflection voltage.

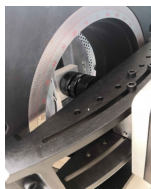


FIGURE 28. Deflection bearing connection.

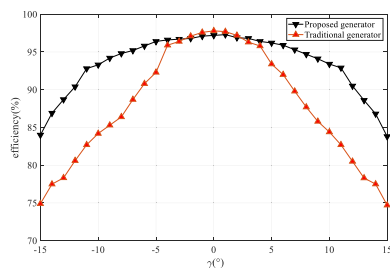


FIGURE 29. Efficiency comparison of two kinds of generators.

deflection angle can effectively improve the voltage efficiency.

Fig. 27. shows the generator experimental setup. By comparing the analytical results with the experimental data, it is found that the maximum five errors are less than 10%. Through comparison, it is found that the analytical method can be used to calculate the voltage waveform quantitatively. As shown in Fig. 27., the prime motor is responsible for simulating wind energy transfer. The generator itself cannot realize the deflection movement, and other auxiliary devices need to be added to help achieve the deflection effect.

The purpose of setting up an experimental platform is to hope to simulate wind energy conversion and verify the principle of this generator. The prototype generator is used to verify the principle. The wind energy simulation of the generator is performed through the prime motor. In practical applications, any auxiliary equipment to help the generator complete the deflection movement can also be adopted. At the same time, in order to facilitate readers' understanding, the photos at the bearing (as shown in Fig. 28.) are added to more intuitively reflect the structure.

Fig. 29. shows the efficiency comparison of the two types of generators. The deflection type double stator switched reluctance generator has higher efficiency in different wind directions. It can be seen that the deflectable dual-stator switched reluctance generator has a very stable efficiency

overall, which is not achieved by traditional generators, and is also the main advantage of this generator.

We obtain the voltage characteristic curve of the generator through an oscilloscope and record the data at the same time. Then adjust the prime mover to deflect the DDSRG to a certain angle, then use the oscilloscope to retest and record the voltage value of the DDSRG.

VI. CONCLUSION

In this article, a deflection type switched reluctance generator with two stators is proposed, and the model of the generator is introduced. At the same time, the modeling of the voltage characteristics of the generator electrode is analyzed. The accuracy of the research is illustrated by comparing the experimental data with the analytical data. In this work, "integral difference" can be used to measure the deviation degree of two curves with the same change rule but larger or smaller amplitude, and can also be used to quantitatively describe the deviation degree. The smaller the "integral difference", the higher the fit of the two curves, and it also shows that the theory is closer to the experiment. At the same time, it has been verified that this generator does have the characteristics of high-efficiency power generation. By comparing the analytical method with the experimental data, it can be concluded that the analytical method has a better prediction accuracy for voltage characteristics. At the same time, the research shows that the generator with deflection structure can better adapt to different wind directions, and has better power generation characteristics compared with the generator with traditional structure. Through actual measurement, It can be verified through experiments that the efficiency of the generator is increased by 5~8% every time the wind direction and turbine offset angle are reduced by 5°.

REFERENCES

- [1] Y. Chen, X. Zhu, L. Quan, X. Han, and X. He, "Parameter Sensitivity Optimization Design and Performance Analysis of Double-Salient Permanent-Magnet Double-Stator Machine," *Trans. China Electrotech. Soc.*, vol. 32, no. 8, pp. 160–168, Apr. 2017.
- [2] Y. Zhou and Y. Sun, "A double-stator type bearingless switched reluctance dual-channel full-period generator," *Proc. CSEE.*, vol. 35., no. 91, pp. 2295–2303, May 2015.
- [3] L. García-Tabarés, "New type of linear switched reluctance generator for wave energy applications," *IEEE Trans. Appl. Supercond.*, vol. 30, no. 4, pp. 1–5, Jun. 2020, Art. no. 5207105.
- [4] X. Sun, K. Diao, G. Lei, Y. Guo, and J. Zhu, "Study on segmented-rotor switched reluctance motors with different rotor pole numbers for BSG system of hybrid electric vehicles," *IEEE Trans. Veh. Technol.*, vol. 68, no. 6, pp. 5537–5547, Jun. 2019.
- [5] H. Chen, D. Xu, and X. Deng, "Control for power converter of small-scale switched reluctance wind power generator," *IEEE Trans. Ind. Electron.*, early access, Mar. 11, 2020, doi: 10.1109/TIE.2020.2978689.
- [6] V. S. de Castro Teixeira, E. R. Filho, T. A. dos Santos Barros, and A. B. Moreira, "Design, optimization and analysis of the axial C-core switched reluctance generator for wind power application," in *Proc. Int. Conf. Renew. Energy Res. Appl. (ICRERA)*, Palermo, Italy, 2015, pp. 833–837.
- [7] D. Wang, C. Shao, X. Wang, and C. Zhang, "Performance characteristics and preliminary analysis of low cost tubular linear switch reluctance generator for direct drive WEC," *IEEE Trans. Appl. Supercond.*, vol. 26, no. 7, Oct. 2016, Art. no. 0612205.
- [8] X. Liu, K. Park, and Z. Chen, "A novel excitation assistance switched reluctance wind power generator," *IEEE Trans. Magn.*, vol. 50, no. 11, Dec. 2014, Art. no. 8203304.

- [9] V. S. De Castro Teixeira, T. A. D. S. Barros, A. B. Moreira, and E. R. Filho, "Methodology for the electromagnetic design of the axial-flux C-core switched reluctance generator," *IEEE Access*, vol. 6, pp. 65463–65473, 2018.
- [10] N. Arbab, W. Wang, C. Lin, J. Hearron, and B. Fahimi, "Thermal modeling and analysis of a double-stator switched reluctance motor," *IEEE Trans. Energy Convers.*, vol. 30, no. 3, pp. 1209–1217, Sep. 2015.
- [11] A. H. Isfahani and B. Fahimi, "Comparison of mechanical vibration between a double-stator switched reluctance machine and a conventional switched reluctance machine," *IEEE Trans. Magn.*, vol. 50, no. 2, pp. 293–296, Feb. 2014, doi: 10.1109/TMAG.2013.2286569.
- [12] M. Asgar and E. Afjei, "Radial force reduction in a new flat-type double-stator switched reluctance motor," *IEEE Trans. Energy Convers.*, vol. 31, no. 1, pp. 141–149, Mar. 2016.
- [13] W. Wang, M. Luo, E. Cosoroaba, B. Fahimi, and M. Kiani, "Rotor shape investigation and optimization of double stator switched reluctance machine," *IEEE Trans. Magn.*, vol. 51, no. 3, Mar. 2015, Art. no. 8103304.
- [14] Y. Liu, S. Niu, S. L. Ho, W. N. Fu, and T. W. Ching, "Design and analysis of a new HTS double-stator doubly fed wind generator," *IEEE Trans. Appl. Supercond.*, vol. 25, no. 3, Jun. 2015, Art. no. 5200804.
- [15] Z. Q. Jiang, J. P. Hu, R. Ye, and J. X. Jin, "Field coil optimization and characteristics contrastive analysis for a high-temperature superconducting generator prototype," *IEEE Trans. Appl. Supercond.*, vol. 28, no. 5, Aug. 2018, Art. no. 5206207.
- [16] P. Y. Grachev, A. S. Tabachinskiy, and P. Kanagavel, "New stator construction and simulation of high-efficiency wind turbine generators," *IEEE Trans. Ind. Appl.*, vol. 56, no. 2, pp. 1389–1396, Mar. 2020.
- [17] H. Yahia, R. Dhifaoui, and N. Liouane, "Differential evolution method-based output power optimisation of switched reluctance generator for wind turbine applications," *IET Renew. Power Gener.*, vol. 8, no. 7, pp. 795–806, Sep. 2014.
- [18] H.-U. Shin and K.-B. Lee, "Optimal design of a switched reluctance generator for small wind power system using a genetic algorithm," in *Proc. 9th Int. Conf. Power Electron. ECCE Asia (ICPE-ECCE Asia)*, Jun. 2015, pp. 2209–2214.
- [19] K. Diao, X. Sun, G. Lei, Y. Guo, and J. Zhu, "Multiobjective system level optimization method for switched reluctance motor drive systems using finite-element model," *IEEE Trans. Ind. Electron.*, vol. 67, no. 12, pp. 10055–10064, Dec. 2020.
- [20] A. M. Omekanda, "Robust torque and torque-per-inertia optimization of a switched reluctance motor using the taguchi methods," *IEEE Trans. Ind. Appl.*, vol. 42, no. 2, pp. 473–478, Mar. 2006.
- [21] Z. Zhang, S. Rao, and X. Zhang, "Performance prediction of switched reluctance motor using improved generalized regression neural networks for design optimization," *CES Trans. Electr. Mach. Syst.*, vol. 2, no. 4, pp. 371–376, Dec. 2018.
- [22] G.-Z. Cao, J.-L. Fang, S.-D. Huang, J.-A. Duan, and J. F. Pan, "Optimization design of the planar switched reluctance motor on electromagnetic force ripple minimization," *IEEE Trans. Magn.*, vol. 50, no. 11, Nov. 2014, Art. no. 8203404.
- [23] C. Ma and L. Qu, "Multiobjective optimization of switched reluctance motors based on design of experiments and particle swarm optimization," *IEEE Trans. Energy Convers.*, vol. 30, no. 3, pp. 1144–1153, Sep. 2015.
- [24] V. Rallabandi, J. Wu, P. Zhou, D. G. Dorrell, and D. M. Ionel, "Optimal design of a switched reluctance motor with magnetically disconnected rotor modules using a design of experiments differential evolution FEA-based method," *IEEE Trans. Magn.*, vol. 54, no. 11, Nov. 2018, Art. no. 8205705.
- [25] Z. Li, Q. Chen, and Q. Wang, "Analysis of multi-physics coupling field of Multi-Degree-of-Freedom permanent magnet spherical motor," *IEEE Trans. Magn.*, vol. 55, no. 6, Jun. 2019, Art. no. 8201505.
- [26] X. Yu, F. Yang, L. Ou, Q. Xu, and W. Zhang, "Two-degree-of-freedom optimal consensus scheme of fractional-order multi-agent systems," *IET Control Theory Appl.*, vol. 12, no. 16, pp. 2175–2183, Nov. 2018.
- [27] S. Cho, J.-S. Lim, Y. J. Oh, G. Jeong, D.-W. Kang, and J. Lee, "A study on output characteristics of the spherical multi-DOF motor according to the number of phases and pole pitch angles," *IEEE Trans. Magn.*, vol. 54, no. 11, Nov. 2018, Art. no. 8205005.
- [28] H.-S. Hong, S.-H. Won, H.-W. Lee, J.-N. Bae, and J. Lee, "Design of torque actuator in hybrid multi-DOF system considering magnetic saturation," *IEEE Trans. Magn.*, vol. 51, no. 11, Nov. 2015, Art. no. 8208204.
- [29] Z. Li, Q. Lun, D. Xing, and P. Gao, "Analysis and implementation of a 3-DOF deflection-type PM motor," *IEEE Trans. Magn.*, vol. 51, no. 11, Nov. 2015, Art. no. 8207304.
- [30] L. Gan, Y. Pei, and F. Chai, "Tilting torque calculation of a novel tiered type permanent magnet spherical motor," *IEEE Trans. Ind. Electron.*, vol. 67, no. 1, pp. 421–431, Jan. 2020.



ZHENG LI (Member, IEEE) was born in Shijiazhuang, Hebei, China, in 1980. He received the B.Sc. and Ph.D. degrees in electrical engineering and power electronics and electric drive from the Hefei University of Technology, Hefei, China, in 2002 and 2007, respectively

Since 2007, he has been a Lecturer, an Associate Professor, and a Professor with the School of Electrical Engineering, Hebei University of Science and Technology. From July 2013 to July 2014,

he was a Visiting Scholar and part-time Faculty Member with the College of Engineering, Wayne State University, USA. He is the author of more than 160 published articles. His current research interests include design, analysis, and control of novel motors and actuators, intelligent control, and power electronics.

Dr. Li is an Active Reviewer of the IEEE TRANSACTIONS ON INDUSTRIAL ELECTRONICS, the IEEE TRANSACTIONS ON ENERGY CONVERSION, the IEEE TRANSACTIONS ON MAGNETICS AND ELECTRIC POWER COMPONENTS AND SYSTEMS, and so on.



XUZE YU received the B.Sc. degree in electrical engineering and automation from the Hebei University of Science and Technology, China, Shijiazhuang, in 2017. He is currently a Graduate Student with the Hebei University of Science and Technology. His research interests include the complex motion motor or actuator design and implementation.



ZHE QIAN (Member, IEEE) was born in Xinyang, China, in 1984. He received the B.Sc. and Ph.D. degrees in electrical engineering and power electronics and electric drive from the Hefei University of Technology, Hefei, China, in 2004 and 2012, respectively.

Since 2012, he has been a Lecturer with the School of Electrical Engineering and Automation, Anhui University. His research interest includes special motor design and control.



XUETING WANG received the B.Sc. degree in electrical engineering and automation from the Hebei University of Science and Technology, Shijiazhuang, China, in 2018. She is currently a Graduate Student with the Hebei University of Science and Technology. Her research interests include multi-degree-of-freedom motor design and control.



YU XIAO was born in Chengdu, China, in 1995. He received the bachelor's degree in automation from the Hebei University of Science and Technology, China, in 2018. He is currently a Graduate Student with the Hebei University of Science and Technology. His research interests include special motor control and linear motor drive.



HEXU SUN (Senior Member, IEEE) received the Ph.D. degree in automation from Northeastern University, Shenyang, China, in 1993. He has been a Professor with the School of Control Science and Engineering, Hebei University of Technology, Tianjin, China, and the School of Electrical Engineering, Hebei University of Science and Technology, Shijiazhuang, China. He has authored five books and more than 130 journal articles and conference papers, and holds 13 U.S. patents and five computer software copyrights. His current research interests include robotics and complex engineering systems. He was a recipient of many prestigious national awards from China. He has been the Director in many societies and committees in China. He is currently the invited Plenary Speaker and a General Co-Chair of many international conferences.

...